Appl. Phys. B (2013) 112:441–452
DOI 10.1007/s00340-013-5454-x

Applied Physics B
Lasers and Optics

RAPID COMMUNICATION

A dual-pass Mach–Zehnder interferometer filter using a TCF loop mirror for double-wavelength fiber lasers

Hui Zou · Shuqin Lou · Wei Su · Xin Wang

Received: 5 February 2013 / Accepted: 15 April 2013 / Published online: 7 July 2013

Abstract A dual-pass Mach–Zehnder interferometer filter using a section of twin-core fiber (TCF) loop mirror is proposed. The filter is theoretically and experimentally studied for various interferometer arm difference when TCF length is constant. Theoretical results are validated by the experimental demonstration and in good agreement with the experimental results. And then, by using the filter in a ring fiber laser, a stable and switchable dual-wavelength lasing is obtained experimentally. The 3-dB bandwidth and the SMSR of the output laser are 0.015 nm and higher than 62.4 dB, respectively. The peak power fluctuation and wavelength shift are also monitored to be less than 0.04 dB and 0.02 nm over an hour at room temperature. Furthermore, the output laser can be switched between single and dual wavelength by carefully adjusting the PCs. The experimental results show that the filter can suppress mode competition effectively, improve the SMSR availably, and enhance the stability of the output lasing.

1 Introduction

In recent years, stable and switchable dual-wavelength erbium-doped fiber lasers (EDFL) have attracted much interest. The EDFL is widely applied in optical communications, fiber-optic sensors, and microwave (MW) photonic generation [1–4], because of the inherent characteristic of the EDFL such as stable and tunable lasing wavelength, moderate output peak power, narrow linewidth, high side-mode suppression ratio (SMSR), and good compatibility with other optical fiber components. In order to obtain these properties, wavelength selective filters are very important components which can reduce the mode competition and suppress the mode hopping in the lasers cavity for EDFL. Until now, the main two kinds of optical filters have been proposed to achieve dual-wavelength EDFL [5–12], namely narrow band filters and comb filters. The narrow band filters are usually composed of the fiber Bragg gratings (FBGs) [5–9]. However, the FBG fabrication needs expensive equipments including the phase masks and UV laser [9]. Correspondingly, the comb filters, such as the dual-pass Mach–Zehnder interference filter [10–12], high-birefringence fiber-based Sagnac loop filters [13–15], and the twin-core fiber filter [16, 17], are also introduced into ring cavity fiber laser. These comb filters produce a continuous comb of channels with uniform channel spacing and nearly the same transmissivity. But, this is not helpful to obtain a stable dual-wavelength lasing in EDFL without eliminating the strong homogenous gain broadening of the EDF effectively. Besides, the SMSR of the output laser is less than 55 dB [18]. In order to obtain stable dual-wavelength lasing, developing novel filters with low cost and highly reliable performance is very significant.

In this paper, a dual-pass Mach–Zehnder interferometer filter using a section of TCF loop mirror is proposed. Theoretical and experimental investigations on the characteristics of the filter are carried out in detail. Then, using the filter as a wavelength selector in ring cavity, a stable and switchable dual-wavelength lasing is observed. By adjusting the polarization controllers (PCs), the output laser can be switched between single and dual wavelength at room temperature. Meanwhile, the 3-dB bandwidth and the SMSR of the dual-wavelength laser are 0.015 nm and higher than 62.4 dB, respectively. The power fluctuation

H. Zou · S. Lou (✉) · W. Su · X. Wang
School of Electronic and Information Engineering,
Beijing Jiaotong University, Beijing, China
e-mail: shqlou@bjtu.edu.cn

and wavelength shift are monitored to be less than 0.04 dB and 0.02 nm with intervals at 4 min over an hour at room temperature. The stability and high SMSR of dual-wavelength polarization-maintaining erbium-doped fiber ring laser are achieved due to the introduction of the filter. To the best of our knowledge, it is the first time to propose and demonstrate the filter which is constituted by a dual-pass Mach–Zehnder interferometer filter using a TCF loop mirror and to use it as a wavelength selector in ring cavity.

2 Theoretical analysis and experimental results

The cross-section of the homemade TCF is shown in Fig. 1a. Two cores are arranged at the symmetrical position relative to the central axis of fiber. The refractive index difference of two cores is ~0.89 %, and the distance between the centers of two cores is 14 μm. The diameter of each core is 7 μm. The outer diameter of the TCF is 130 μm. A segment of ~0.48 m TCF is embedded in the loop mirror of the proposed filter as shown in Fig. 1b. The filter is developed from the dual-pass Mach–Zehnder interferometer with a loop mirror which is consisted of a segment of TCF, one 2 × 2 coupler, and two PCs. Two PCs in the loop mirror are used to adjust the state of polarization (SOP) of the circulating light. Two couplers (coupler1 and copler2) are employed to form a dual-pass Mach–Zehnder interferometer with different interferometer arm lengths ($\boldsymbol{L}_1$ and $\boldsymbol{L}_2$). Supposing that the beam (the units light intensity) is launched into the Port 1 of the optical circulator (OC), the input field $\boldsymbol{E}_{1\text{in}}$ with an arbitrary SOP can be decomposed into two orthogonal components E_{1x} and E_{1y} in the x–y plane. Jones vector of the input field $E_{1\text{in}}$ can be represented by

$$[\boldsymbol{E}_{1in}] = \begin{bmatrix} E_{1\text{in}x} \\ E_{1\text{in}y} \end{bmatrix} \tag{1}$$

And the corresponding input light intensity is

$$I_{1\text{in}} = |E_{1x}|^2 + |E_{1y}|^2 \tag{2}$$

After traveling through the coupler1 and coupler2, the electric fields $\boldsymbol{E}_3$ and $\boldsymbol{E}_4$ can be obtained from the following equation.

$$\begin{bmatrix} [\boldsymbol{E}_3] \\ [\boldsymbol{E}_4] \end{bmatrix} = \begin{bmatrix} \sqrt{1-k_2},\ j\sqrt{k_2} \\ j\sqrt{k_2},\ \sqrt{1-k_2} \end{bmatrix} \times \begin{bmatrix} e^{jL_1\beta},\ 0 \\ 0,\ e^{jL_2\beta} \end{bmatrix} \begin{bmatrix} \sqrt{1-k_1},\ j\sqrt{k_1} \\ j\sqrt{k_1},\ \sqrt{1-k_1} \end{bmatrix} \begin{bmatrix} [E_{1in}] \\ 0 \end{bmatrix} \tag{3}$$

In Eq. (3), k_1 and k_2 are the coupling ratios of the coupler1 and the coupler2, respectively. The propagation constant β is denoted by $2\pi n_{\text{eff}}/\lambda$ where n_{eff} is the effective refractive index of the fundamental mode and λ is wavelength in vacuum. After the electric field $\boldsymbol{E}_3$ pass through PC3, TCF, and PC2 in sequence, the electric field $\boldsymbol{E}_4'$ can be deduced from the transfer matrix

$$[\boldsymbol{E}_4'] = \begin{bmatrix} \cos\theta_2,\ \sin\theta_2 \\ -\sin\theta_2,\ \cos\theta_2 \end{bmatrix} \begin{bmatrix} \sqrt{1-s_2},\ 0 \\ 0,\ \sqrt{s_2} \end{bmatrix} \begin{bmatrix} e^{\frac{jL2\pi n_{\text{eff1}}}{\lambda}},\ 0 \\ 0,\ e^{\frac{jL2\pi n_{\text{eff2}}}{\lambda}} \end{bmatrix} \times \begin{bmatrix} \sqrt{1-s_1},\ 0 \\ 0,\ \sqrt{s_1} \end{bmatrix} \begin{bmatrix} \cos\theta_1,\ \sin\theta_1 \\ -\sin\theta_1,\ \cos\theta_1 \end{bmatrix} [\boldsymbol{E}_3] \tag{4}$$

Analogously, after the electric field $\boldsymbol{E}_4$ traveling through PC2, TCF, and PC3 anticlockwise, the electric field $\boldsymbol{E}_3'$ can be derived from the transfer matrix

$$[\boldsymbol{E}_3'] = \begin{bmatrix} \cos\theta_1,\ -\sin\theta_1 \\ \sin\theta_1,\ \cos\theta_1 \end{bmatrix} \begin{bmatrix} \sqrt{1-s_1},\ 0 \\ 0,\ \sqrt{s_1} \end{bmatrix} \begin{bmatrix} e^{\frac{jL2\pi n_{\text{eff1}}}{\lambda}},\ 0 \\ 0,\ e^{\frac{jL2\pi n_{\text{eff2}}}{\lambda}} \end{bmatrix} \times \begin{bmatrix} \sqrt{1-s_2},0 \\ 0,\sqrt{s_2} \end{bmatrix} \begin{bmatrix} \cos\theta_2,-\sin\theta_2 \\ \sin\theta_2,\cos\theta_2 \end{bmatrix} [\boldsymbol{E}_4] \tag{5}$$

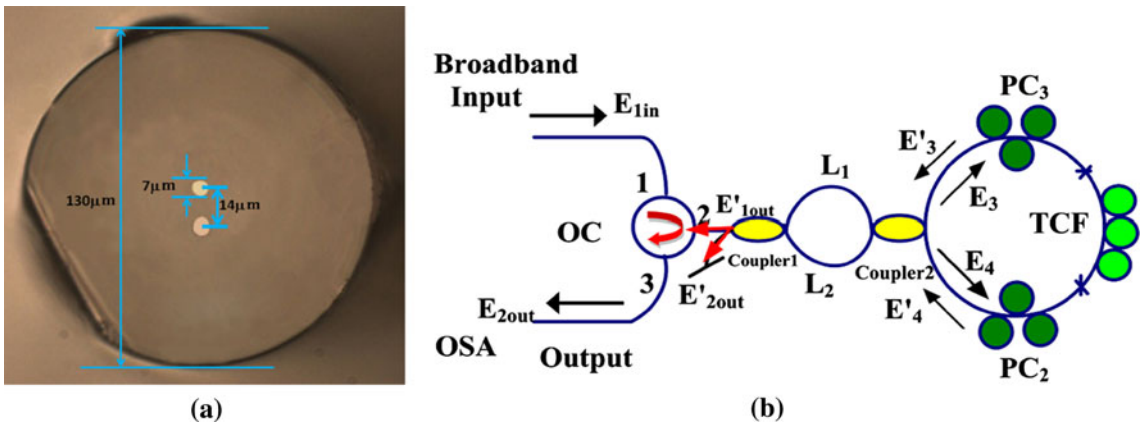

Fig. 1 Micrograph of cross-section of the TCF (**a**). Experimental setup of measuring reflection characters of the proposed filter (**b**)

where θ_1 and θ_2 are the rotation angles of the propagating light through the PC1 and PC2, respectively; n_{effi} ($i = 1$ or 2) is the effective refractive index of the fundamental mode of the two cores in the TCF; $\boldsymbol{\lambda}$is the wavelength in vacuum; $\boldsymbol{s_1}$ and $\boldsymbol{s_2}$ are the power splitting ratios (power from the SMF core splits to both TCF cores); $\boldsymbol{L}$is the length of the TCF. When $\boldsymbol{E_3}'$ and $\boldsymbol{E_4}'$ pass back through two couplers, the output electric field can be written as

$$\begin{bmatrix} [\boldsymbol{E}'_{1\text{out}}] \\ [\boldsymbol{E}'_{2\text{out}}] \end{bmatrix} = \begin{bmatrix} \sqrt{1-k_2},\ j\sqrt{k_2} \\ j\sqrt{k_2},\ \sqrt{1-k_2} \end{bmatrix} \begin{bmatrix} e^{jL_1\beta},\ 0 \\ 0,\ e^{jL_2\beta} \end{bmatrix} \times \begin{bmatrix} \sqrt{1-k_1},\ j\sqrt{k_1} \\ j\sqrt{k_1},\ \sqrt{1-k_1} \end{bmatrix} \begin{bmatrix} [\boldsymbol{E}'_3] \\ [\boldsymbol{E}'_4] \end{bmatrix} \tag{6}$$

The final output $\boldsymbol{E}_{2\text{out}}$ is equal to the electric field $\boldsymbol{E}'_{1\text{out}}$ due to the use of the optical circulator. Thus, the final light intensity in the port 3 of the OC can be deduced as

$$I_{2\text{out}} = |E_{\text{out}2x}|^2 + |E_{\text{out}2y}|^2 \tag{7}$$

From Eqs. (1) to (7), we can obtain the reflectivity function of the novel filter in Fig. 1 as follows:

$$R = \frac{I_{\text{out}2}}{I_{\text{in}1}} = R_1 R_2 \tag{8}$$

$$\begin{aligned} R_1 = \Big[&(1-k_1)(1-k_2) + k_1 k_2 \\ &-2\sqrt{k_1 k_2 (1-k_1)(1-k_2)}\cos(L_1 - L_2)\beta\Big] \\ &\times \Big[(1-k_1)k_2 + (1-k_2)k_1 \\ &+2\sqrt{k_1 k_2 (1-k_1)(1-k_2)}\cos(L_1 - L_2)\beta\Big] \end{aligned} \tag{9}$$

$$\begin{aligned} R_2 = \Big\{&(2s_1 s_2 - s_1 - s_2 + 1)\sin^2(\theta_1 - \theta_2) \\ &+ s_1 s_2 \big[4\cos^2\theta_1 \cos^2\theta_2 + 4\sin^2\theta_1 \sin^2\theta_2 \\ &+ 4\sin(\theta_1 - \theta_2)\cos(\theta_1 + \theta_2)\big] + (1 - s_1)(1 - s_2) \\ &\times \big[4\cos^2\theta_1 \cos^2\theta_2 + 4\sin^2\theta_1 \sin^2\theta_2 \\ &- 4\sin(\theta_1 - \theta_2)\cos(\theta_1 + \theta_2)\big] \\ &- 2\sqrt{s_1 s_2 (1 - s_1)(1 - s_2)}\big[\sin 2\theta_1 \sin 2\theta_2 \\ &+ 4\sin^2(\theta_1 - \theta_2)\big]\cos\frac{2\pi L(n_{\text{eff}1} - n_{\text{eff}2})}{\lambda}\Big\} \end{aligned} \tag{10}$$

In order to give an explanation in detail, the reflectivity function R in Eq. (8) is divided into two parts R_1 and R_2, which are represented by Eqs. (9) and (10), respectively. In Eq. (9), R_1 is determined by the coupling ratios of the two couplers (coupler1 and coupler2) and the difference of two interferometer arms length of the dual-pass Mach–Zehnder interferometer ($\boldsymbol{\Delta L} = \boldsymbol{L}_1$–$\boldsymbol{L}_2$). Meanwhile, in Eq. (10), R_2 is related to the two power splitting ratios ($\boldsymbol{s_1}$ and $\boldsymbol{s_2}$), the length of the TCF (L), and the rotation angles of the propagating light through the PCs (θ_1 and θ_2).

It can be seen from Eq. (8) that R is equal to R_1 when $R_2 = 1$ (the TCF is not connected to the filter). The filter can act as a double-pass Mach–Zehnder comb filter with the path difference $\boldsymbol{\Delta L}$. Figure 2a shows the theoretical result of the double-pass Mach–Zehnder comb filter with $\boldsymbol{\Delta L}$ = ~1.56 cm. The comb spacing of 0.054 nm can be obtained from the theoretical simulation.

A broadband optical source is connected to port1 of the OC to provide an injected beam of light, and an optical spectrum analyzer (OSA, YOKOGAWA, and AQ6370C) with spectral resolution of 0.02 nm is connected to port3 of the OC to detect the reflected spectra of the filter. The corresponding experimental result is shown in Fig. 2b.

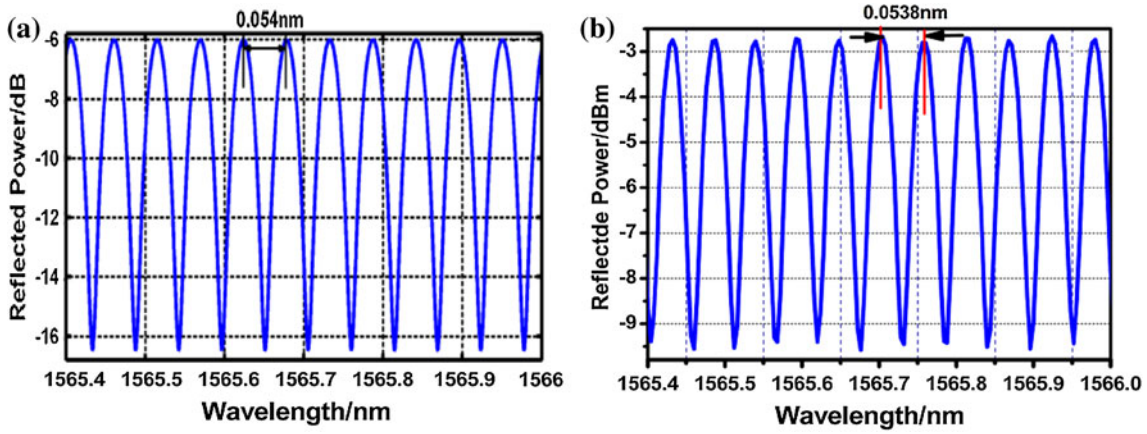

Fig. 2 Simulation results (**a**) and experimental results (**b**) of reflectivity spectra of the R_1

The comb wavelength spacing in experiment is 0.0538 nm which is approximate to the theoretical result.

When $R_1 = 1$ (the double-pass Mach–Zehnder interference is not connected to the filter), R is equal to R_2 which is related to the length of the TCF, that is, $\boldsymbol{L}(L = 0.48$ m) and the filter acts as the TCF comb filter. In order to reduce the insertion loss and couple the light from SMF to the two core of TCF as much as possible, we splice the SMF and TCF along the axial direction by programming the fusion procedures and fusion parameters of the commercial fusion splicer (Fujikura Corporation, mode FCM-50S) and taper the splice regions between SMF and

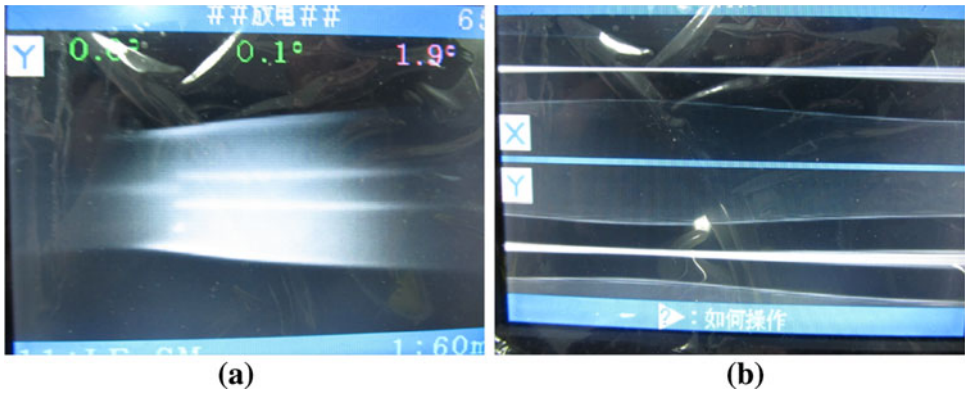

Fig. 3 The fusion image (**a**) of SMF (*left*) and TCF (*right*) and tapering image (**b**) of SMF (left) and TCF (*right*)

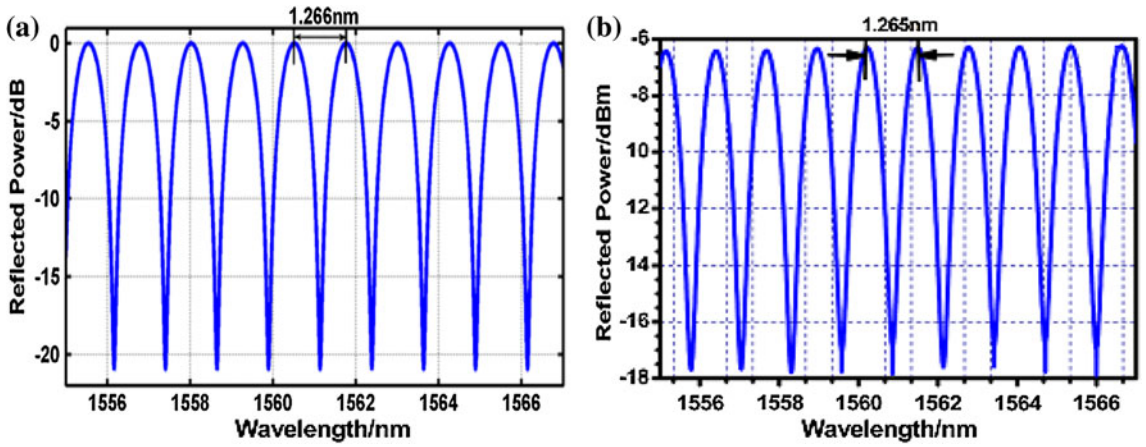

Fig. 4 Simulation result (**a**) and experimental measure (**b**) reflectivity spectra of R_2

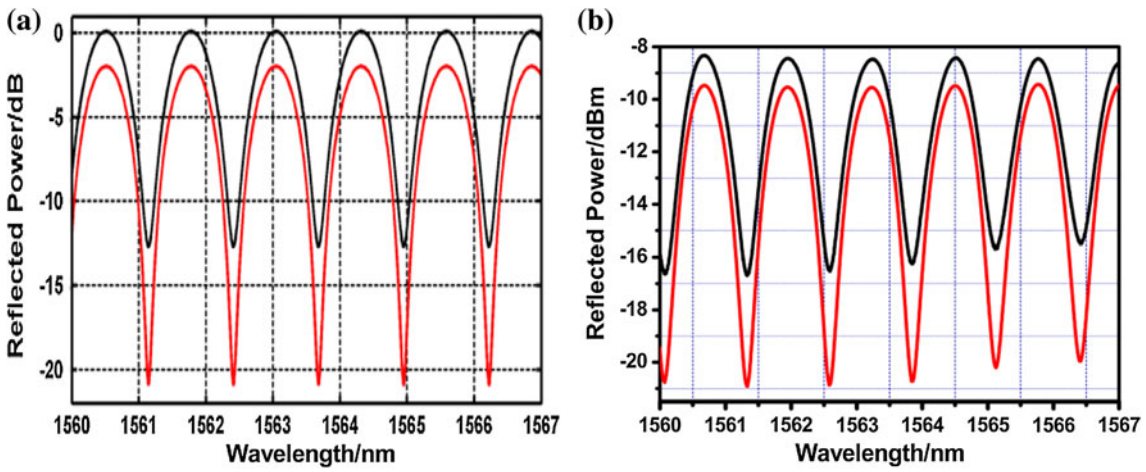

Fig. 5 Simulation result (**a**) and experimental measure (**b**) of reflectivity spectra of R_2 with the different PCs' states

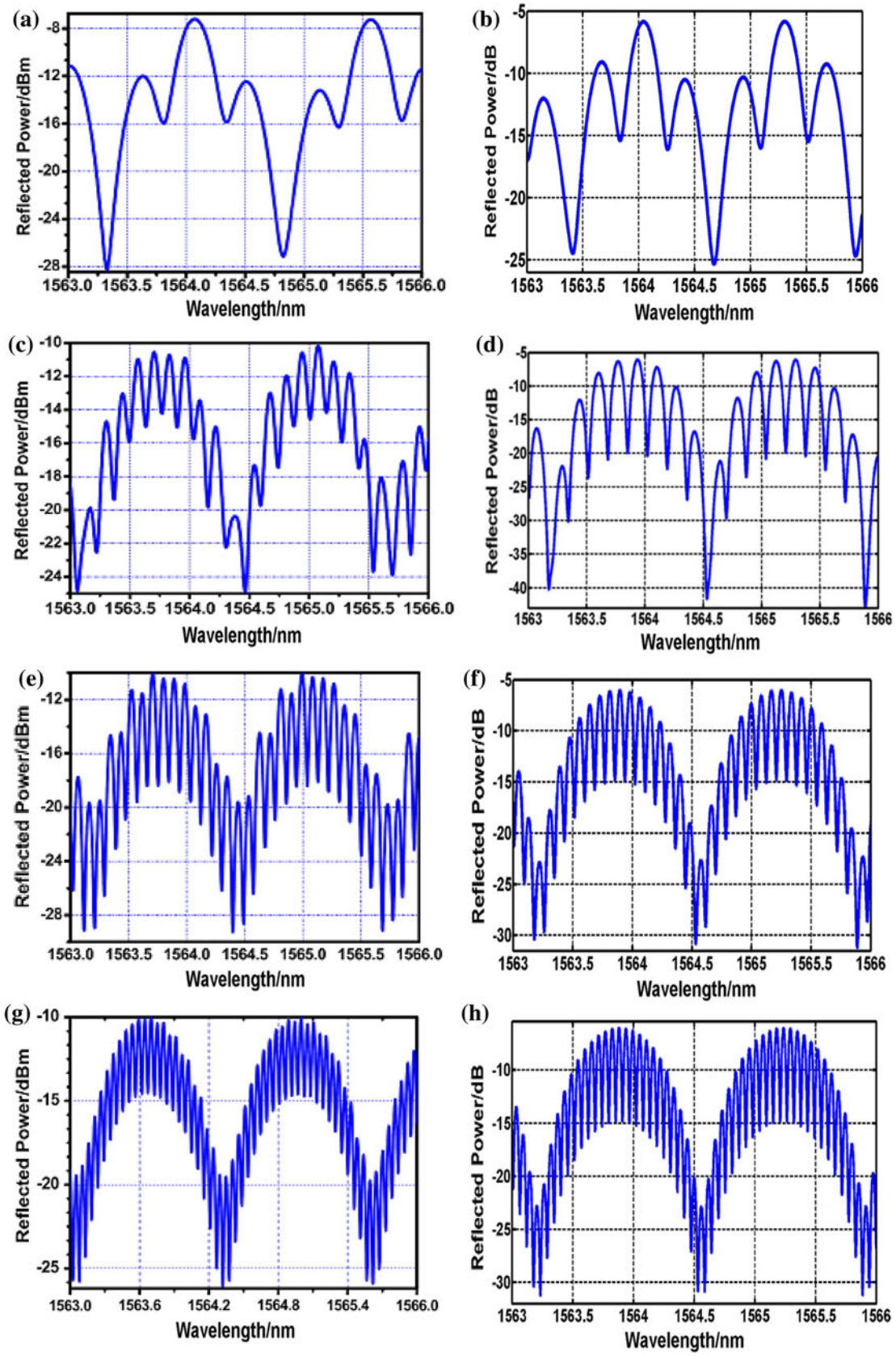

Fig. 6 The reflectivity spectra of experimental results (*Left column*) and numerical simulation (*Right column*) of the filter with different ΔL of 0.25 cm (**a**, **b**), 0.5 cm (**c**, **d**), 1 cm (**e**, **f**), 1.5 cm (**g**, **h**), 2 cm (**i**, **j**), 2.5 cm (**k**, **l**)

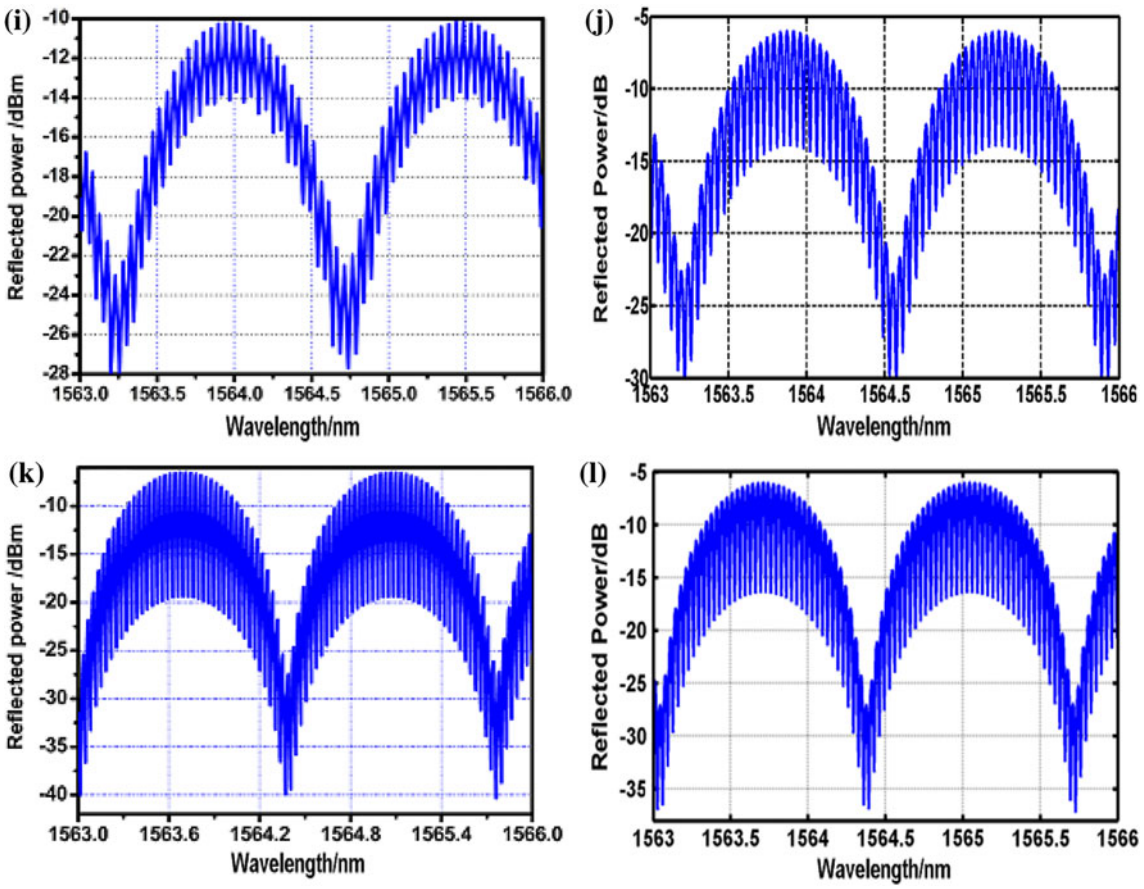

Fig. 6 continued

TCF, as shown in Fig. 3. Through changing the taper parameters in fusion splicer, we optimize the tapered length. As a result, the light of SMF-in can be expanded at the first taper and thus more power from SMF-in is coupled to two cores of the TCF as averagely as possible [19]. When the beam of light propagates through the left-splice point between the TCF and SMF, a part of light from the left SMF can be coupled to the two cores of the TCF. When the light from the two cores of TCF converges at the right-splice point and then interference effect occurs due to different refractive indices of dual cores. So, the beam of light from SMF is coupled to the two cores of the TCF on average [12], we set the values of the power splitting ratio s_1 and s_2 both at 0.5 theoretically. The reflectivity spectra of theory and experiment are shown in Fig. 4. Compared with the theoretical result in Fig. 4a, the experimental reflectivity spectra in Fig. 4b are nearly in good agreement with the theoretical result. Figure 5 shows the reflectivity spectra of the filter under different SOPs by adjusting the PCs, which are corresponding to the theoretical polarization states: $\theta_1 = -0.5\pi$, $\theta_2 = -0.025\pi$ and $\theta_1 = -0.5\pi$, $\theta_2 = -0.009\pi$. It can be found from Fig. 5 that the changes of polarization states have distinct effect on the extinction ratio of the filter, but have slight effect on the wavelength of reflection peak.

When $R_1 \neq 1$ and $R_2 \neq 1$, we investigate the characteristics of the filter at the following parameters: $k_1 = 0.5$, $k_2 = 0.5$, $L = 0.48$ m, $n_{\text{eff1}} - n_{\text{eff2}} = 0.00408$, $s_1 = 0.5$, $s_2 = 0.5$. Here, we concentrate on the reflectivity properties of the filter with different ΔL of MZI and SOP of PCs.

Firstly, we change the values of ΔL ($\Delta L = 0.25, 0.5, 1, 1.5$, 2, and 2.5 cm), and the reflectivity spectra of the proposed filter are shown in Fig. 6. It can be seen from Fig. 6 that the reflected spectrum has one big envelope peak which including small multi-peaks with nearly same wavelength spacing. With the increase in the length of ΔL, the number of small multi-peaks in each envelope peak increases distinctly and the corresponding wavelength spacing of the adjacent small multi-peaks decreases. However, the wavelength spacing of the adjacent big envelope peak does not vary with the change of ΔL. These results can be explained by the influence of two different filters: the double-loop Mach–Zehnder comb filter and the TCF comb filter. Small multi-peaks in each envelope peak are produced by the double-loop Mach–Zehnder interference. So the wavelength spacing of the adjacent small multi-peaks is sensitive to the ΔL of MZI. When we change

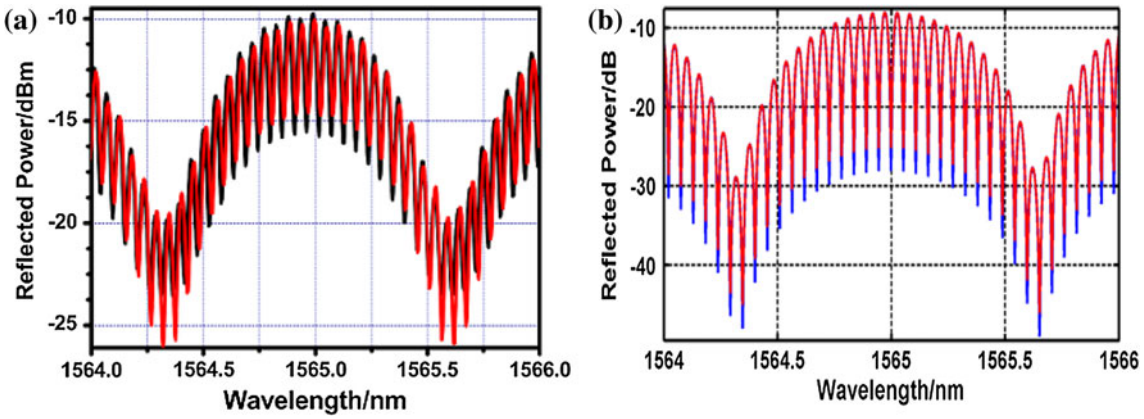

Fig. 7 Experimental measuring (**a**) and simulation results (**b**) of reflectivity spectra of the novel filter different PCs' states

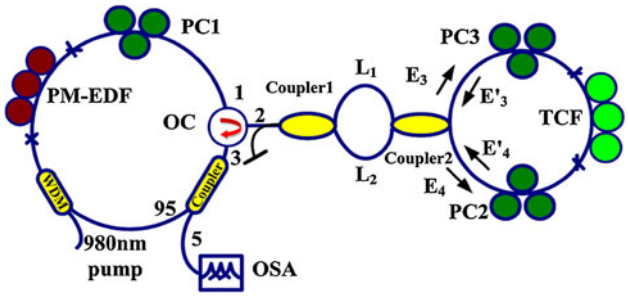

Fig. 8 Schematic of the proposed stable switchable dual-wavelength polarization-maintaining erbium-doped fiber ring laser using the novel filters

ΔL from 0.25 to 2.5 cm, the corresponding wavelength spacing changes from 1.45 to 0.034 nm. Experimental results are in accordance with the correspondingly theoretical results. While the big envelope peak is caused by the TCF filter, thus the wavelength spacing of the big envelope peak is determined by the length of the TCF. And the wavelength spacing of the adjacent big envelope peak keeps constant during the change of ΔL. The final reflectivity spectra of novel filter are overlapped by the reflectivity spectra of TCF filter and the double-loop Mach–Zehnder comb filter.

Then, when the SOP is altered by adjusting PCs, the extinction ratio of the filter is changed correspondingly. But the wavelength of reflection peak keeps constant as shown in Fig. 7. By adjusting the PCs, the characteristic of the polarization dependence is introduced and then different wavelengths can get different gain and loss. As a result, the spectrum hole burning effect is aroused and the stability of output wavelength is improved in ring cavity fiber laser.

3 Experimental results of dual-wavelength fiber laser

Introducing the filter into the ring cavity, we proposed a stable and switchable dual-wavelength polarization-maintaining erbium-doped fiber (PM-EDF) ring laser as shown in Fig. 8. In the fiber ring cavity, there are a segment of 2.5 m PM-EDF serving as the gain medium, a 1,550/980 nm WDM used to couple the 980 nm laser with 250 mW maximum output as the co-propagating pump into the PM-EDF, PC1 employed to adjust the switchable laser output, an optical circulator used to form a unidirectional ring and connect the novel filter, and a 95/5 fiber coupler as the laser output. The output lasing is monitored by the OSA from the 5 % port of 95/5 coupler.

The aim of using the filter is to alleviate the mode competition and improve the stable performance of the erbium-doped fiber laser (EDFL). At an incident pump power of 200 mW, we have acquired six output spectra of single-wavelength lasing by adjusting the PCs, which are corresponding to the situation at different arm length ΔL, as shown in Fig. 9. For each situation, the 3-dB bandwidths and the SMSRs of the lasing wavelength are measured. It can be seen from Fig. 9 that the maximum SMSR reaches to 67.76 dB and the narrowest 3-dB bandwidth of 0.0150 nm is obtained when $\Delta L = 1.5$ cm. This phenomenon can be attributed to the role of small multi-wavelength peaks which can lower mode hopping and suppress the mode competition in ring laser. When a small peak wavelength lies in the peak of the big envelope, it is easy to be lased due to its high gain and low loss. And then high SMSR and narrow 3-dB bandwidth can be achieved, while other little peak wavelengths are suppressed due to the spectrum hole burning of the ring laser cavity.

To investigate the power and wavelength stability, the output spectra are monitored for an hour with the interval of four minutes at room temperature in Fig. 10. Obviously, the fluctuation of the maximum peak power and wavelength shift is 0.06 dB and 0.02 nm, respectively.

By carefully adjusting PCs, we can obtain stable dual-wavelength lasing with the pump power of 200 mW at room temperature, as shown in Fig. 11. The dual wavelength is located at 1,560.05 and 1,559.89 nm and their

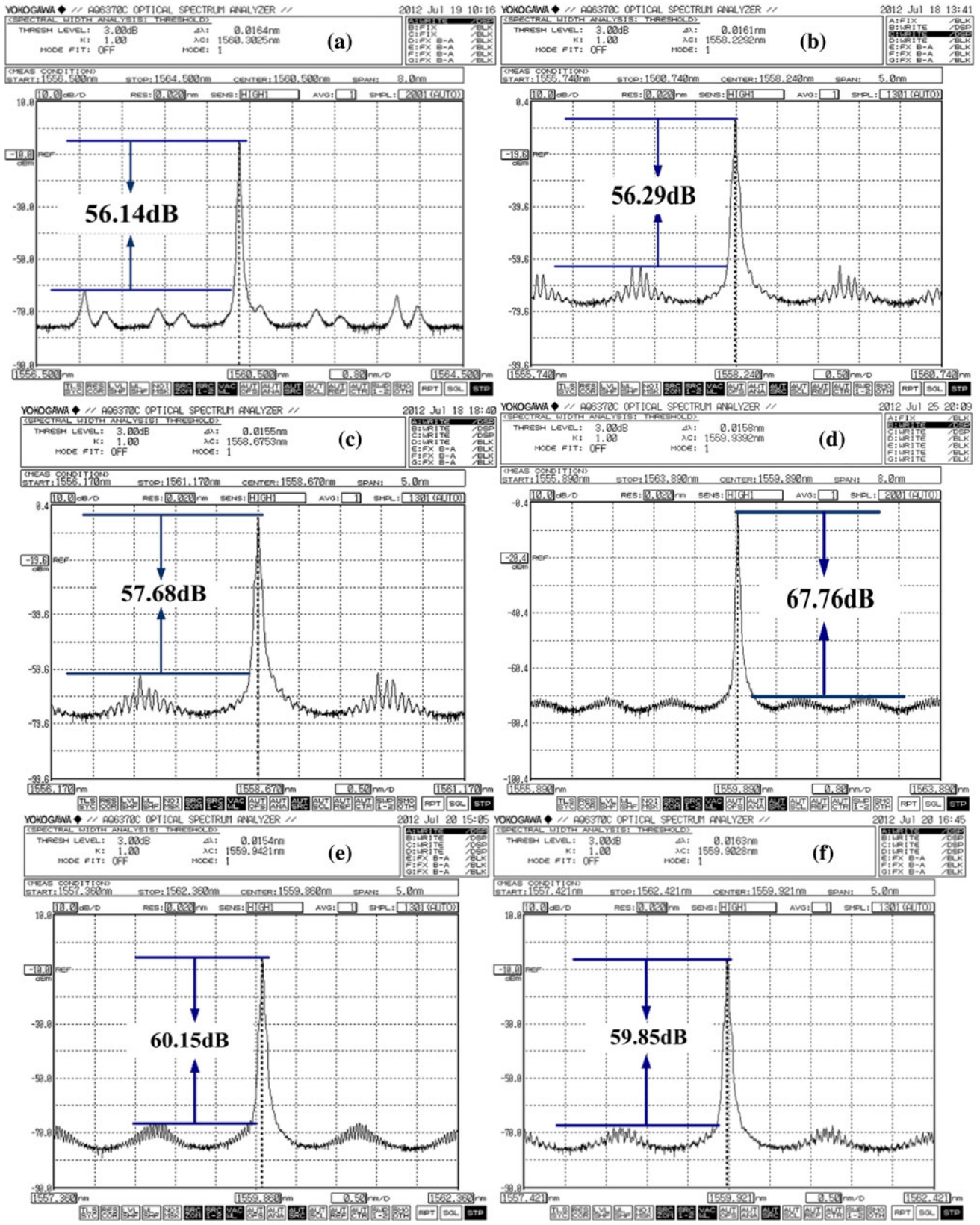

Fig. 9 Measured output spectrum of single-wavelength lasing using the novel filter with different ΔL: **a** $\Delta L = 0.25$ cm, **b** $\Delta L = 0.5$ cm, **c** $\Delta L = 1$ cm, **d** $\Delta L = 1.5$ cm, **e** $\Delta L = 2$ cm, **f** $\Delta L = 2.5$ cm

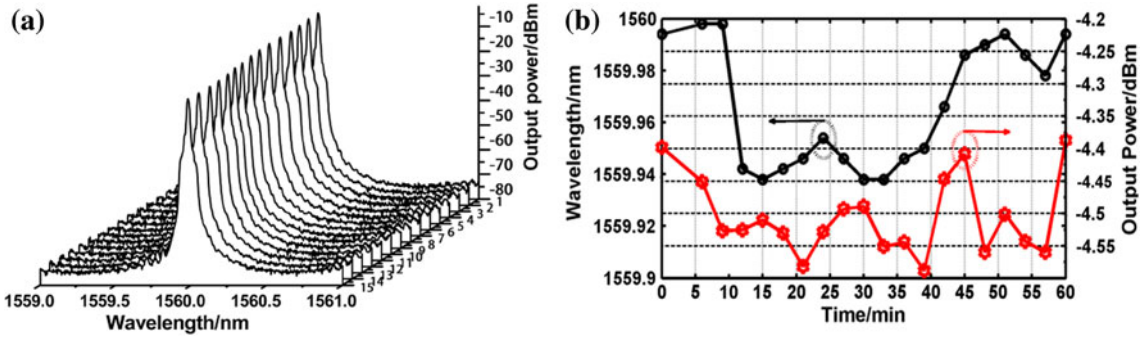

Fig. 10 **a** Measured output spectrum at fixed center wavelength of 1559.98 nm at every 4 min. **b** Fluctuations of the output wavelength and output power over a period of 60 min

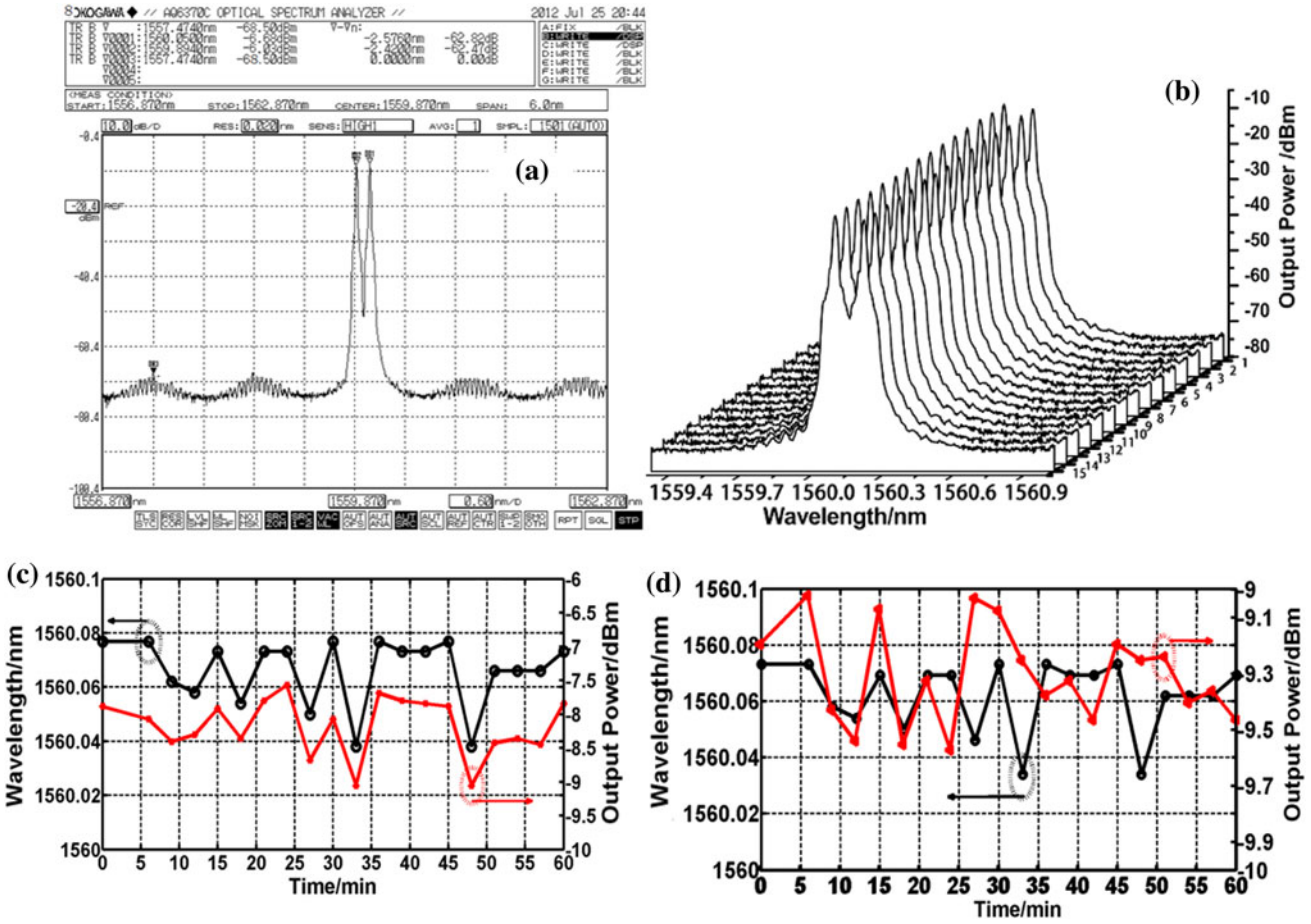

Fig. 11 **a** Output spectra of two lasing center wavelengths at 1560.05 and 1559.89 nm. **b** Repeated scanning spectrum with a time interval of 4 min for an hour. Fluctuations of the output wavelength and power with time at the fixed wavelength of 1560.05 nm (**c**) and 1559.89 nm (**d**)

SMSRs are higher than 62.4 dB. The stability tests on the dual-wavelength output are also carried out and monitored by recording the spectra with the interval of every four minutes for an hour as shown in Fig. 11b. The corresponding peak power fluctuation and the wavelength shift are summarized in Fig. 11c, d. It can be seen from Fig. 11c, d that the maximum peak power fluctuation and the wavelength shift are $\sim$0.35 dB and $\sim$0.02 nm, respectively. By using the filter, a stable dual-wavelength lasing at room temperature is achieved. This can be explained by the PHB effect which is enhanced by adjusting the SOP of PCs. Due to the birefringence existing in TCF [20], the phase difference between the fast and slow axis is different for various wavelengths in TCF. As a

result, the TCF loop mirror provides different polarization rotations for various wavelengths, as shown in Figs. 5 and 7. So the polarization states of different wavelengths are diversified. The light with a certain polarization orientation in rare earth-doped fiber only consumes the upper energy ions relevant with this orientation, and thus PHB is greatly enhanced. In addition, polarization-dependent gain can be further enhanced for various wavelengths due to the use of PM-EDF. This can also enhance PHB effects. As a result, the homogeneous broadening of EDF is reduced, the mode competition is eliminated, and stable dual-wavelength oscillation at room temperature is established [21–23]. As a result, the homogenous gain broadening of EDF is greatly weakened and the wavelength competition is also reduced [5]. Hence, it is possible to obtain a stable and switchable dual-wavelength lasing at room temperature using the filter.

In order to further verify the significance of the filter for selecting lasing wavelength in the ring cavity, two reference experiments in the same ring cavity are carried out. Firstly, using the only TCF as a filter ($\boldsymbol{L} = 0.48$ m) to select lasing wavelength in Fig. 12a, at an incident pump power of 200 mW, the lasing at the wavelength of 1,560.51 nm is obtained in Fig. 12b. The 3-dB bandwidth and SMSR are 0.0483 nm

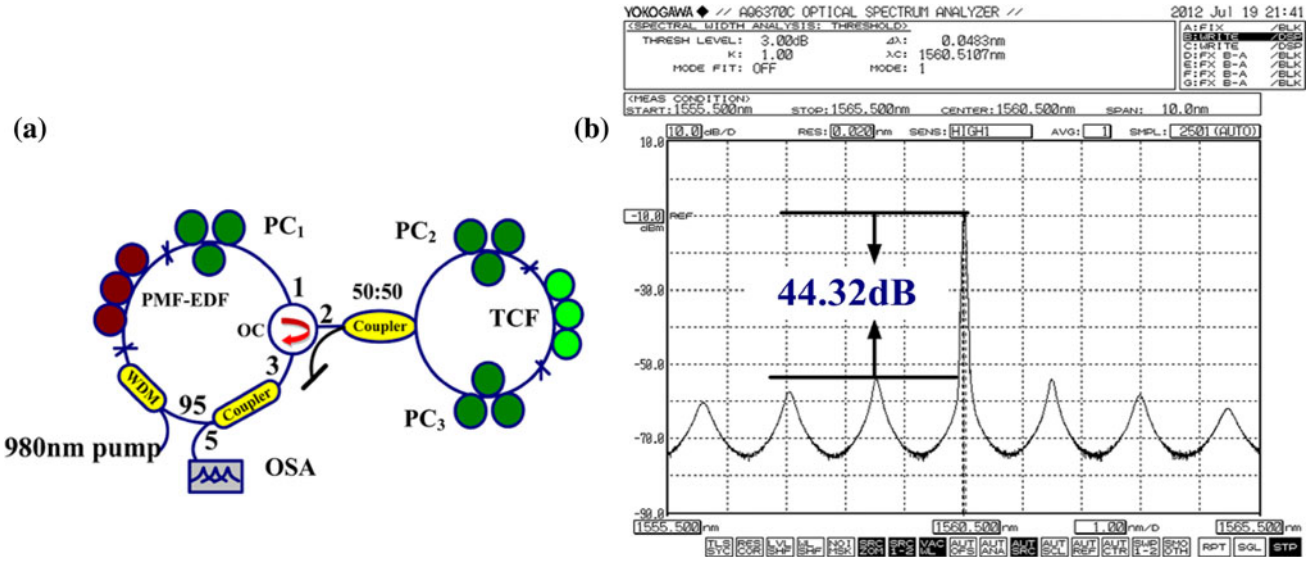

Fig. 12 **a** Schematic diagram of the ring cavity fiber laser only using the TCF as a filter and **b** its output spectra of the wavelength lasing at 1560.51 nm

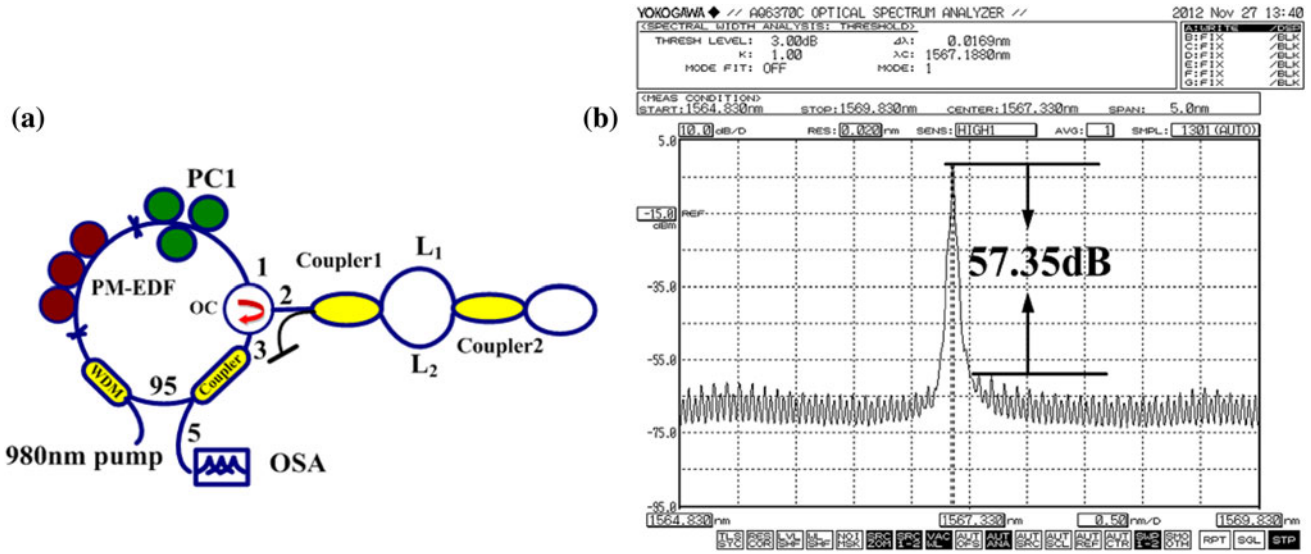

Fig. 13 Schematic diagram of the ring cavity fiber laser only using the dual-pass Mach–Zehnder interference as a filter (**a**) and its output spectra of the lasing centered at 1567.1880 nm (**b**)

and 44.32 dB, respectively. Then, the dual-pass Mach–Zehnder interference ($\Delta L = 1.5$ cm) as filter to select the lasing wavelength alone in the same ring cavity is taken in Fig. 13a, and the lasing at the wavelength of 1,560.51 nm is observed in Fig. 13b when the incident pump power is set at 200 mW. The 3-dB bandwidth and SMSR are 0.0169 nm and 57.35 dB, respectively. The above two reference experiments demonstrate that the ring cavity of PM-EDFL with the proposed filter can achieve higher performance than that with only the TCF comb filter or the dual-pass Mach–Zehnder comb filter.

4 Conclusions

In conclusion, we propose and successfully fabricate the filter based on a dual-loop Mach–Zehnder interferometer using a TCF loop mirror, whose characteristics are analyzed theoretically and experimentally confirmed. By using the filter in the ring fiber laser as a wavelength selector, a stable and switchable dual-wavelength lasing is obtained experimentally. By adjusting the PCs, the output laser can be switched between single and dual wavelength at room temperature. The 3-dB bandwidth and the SMSR of the dual-wavelength output laser are 0.015 nm and higher than 62.4 dB, respectively. The peak power fluctuation and wavelength shift are monitored to be less than 0.35 dB and 0.02 nm, respectively. Compared with the same ring cavity with only the TCF or the dual-pass Mach–Zehnder interferometer as a wavelength selector, the lasing wavelength with the filter has the superior performance with narrower 3-dB bandwidth and higher SMSR. In addition, low cost and high stability make this ring laser with novel filter a potential candidate in optical communication system, optical fibers sensors, especially in microwave (MW) photonics system.

Acknowledgments This work is supported by the National Natural Science Foundation of China under Grant Nos. 61177082 and 61205074, Beijing Natural Science Foundation under Grant No. 4122063.

References

1. L. Talaverano, S. Abad, S. Jarabo, M. LOPEZ-Amo, Multi-wavelength fiber laser sources with Bragg-grating sensor multiplexing capability. J. Lightwave Technol. **19**(4), 553–558 (2001)
2. Y. Yao, X. Chen, S. Xie, Dual-wavelength erbium-doped fiber laser with a simple linear cavity and its application in microwave generation. IEEE Photonics Technol. Lett. **18**(1), 187–189 (2006)
3. W.S. Liu, M.J. Daru Chen, Sailing He, Dual-wavelength single-longitudinal-mode polarization-maintaining fiber laser and its application in microwave generation. J. Lightwave Technol. **27**(20), 4455–4459 (2009)
4. S. Pan, J.P. Yao, A wavelength-switchable single-longitudinal-mode dual-wavelength erbium-doped fiber laser for switchable microwave generation. Opt. Express **17**(7), 5414–5419 (2009)
5. X.M. Liu, X.Q. Zhou, X.F. Tang, J.H. Ng, J.Z. Hao, T.Y. Chai, Edward Leong, C. Lu, Switchable and tunable multi-wavelength erbium-doped fiber laser with fiber Bragg gratings and photonic crystal fiber. IEEE Photonics Technol. Lett. **17**(8), 1626–1628 (2005)
6. X.Y. He, X. Fang, C.R. Liao, D.N. Wang, J.Q. Sun, A tunable and switchable single-longitudinal mode dual-wavelength fiber laser with a simple linear cavity. Opt. Express **17**(24), 21773–21781 (2009)
7. D. Liu, N.Q. Ngo, X.Y. Dong, S.C. Tjin, P. Shum, A stable dual-wavelength fiber laser with tunable wavelength spacing using a polarization-maintaining linear cavity. Applied Physics B **81**, 807–811 (2005)
8. X.Y. He, D.N. Wang, C.R. Liao, Tunable and switchable dual-wavelength single-longitudinal-mode erbium-doped fiber LASERS. J. Lightwave Technol. **29**(6), 842–848 (2011)
9. K.M. Chung, L. Dong, C. Lu, H.Y. Tam, Novel fiber Bragg grating fabrication system for long gratings with independent apodization and with local phase and wavelength control. Opt. Express **19**(13), 12664–12672 (2011)
10. H.L. An, X.Z. Lin, E.Y.B. Pun, H.D. Liu, Multi-wavelength operation of an erbium-doped fiber ring laser using a dual-pass Mach–Zehnder comb filter. Opt. Commun. **169**, 159–165 (1999)
11. A.P. Luo, Z.C. Luo, W.C. Xu, Tunable and switchable multi-wavelength erbium-doped fiber ring laser based on a modified dual-pass Mach-Zehnder interferometer. Opt. Lett. **34**(14), 2135–2137 (2009)
12. F. Wang, E.M. Xu, J.J. Dong, X.L. Zhang, A tunable and switchable single-longitudinal-mode dual-wavelength fiber laser incorporating a reconfigurable dual-pass Mach-Zehnder interferometer and its application in microwave generation. Opt. Commun. **284**(9), 2337–2340 (2011)
13. J.E. Im, B.K. Kim, Y. Chung, Stable SOA-based multi-wavelength fiber ring laser using Sagnac loop mirror incorporating a high-birefringence photonic crystal fiber. Laser Phys. **20**, 1918–1922 (2010)
14. Y.J. Song, L. Zhan, S. Hu, Q.H. Ye, Y.X. Xia, Tunable multi-wavelength brillouin-erbium fiber laser with a polarization-maintaining fiber Sagnac loop filter. IEEE Photon Technol. Letts. **16**(9), 2015–2017 (2004)
15. M. Zhou, Z.Q. Luo, Z.P. Cai, C.C. Ye, Switchable and tunable multiple-channel erbium-doped fiber laser using graphene-polymer nanocomposite and asymmetric two stage fiber Sagnac loop filter. Appl. Opt. **50**, 2490–2498 (2011)
16. H. Zou, S.Q. Lou, G.L. Yin, A wavelength-tunable fiber laser based on a twin-core fiber comb filter. Opt. Laser Technol. **45**, 629–633 (2012)
17. B.K. Kim, Y. Chung, Tunable and switchable SOA-based multi-wavelength fiber laser using twin-core photonic crystal fiber. Laser Phys. Lett. **9**(10), 734–738 (2012)
18. M.A. Ummy, N. Madamopoulos, M. Razani, A. Hossain, R. Dorsinville, Switchable dual-wavelength SOA-based fiber laser with continuous tunability over the C-band at room-temperature. Opt. Express **20**(21), 23367–23373 (2012)
19. X.L. Zhu, L.B. Yuan, Z.H. Liu, J. Yang, C.Y. Guan, Coupling theoretical mode between single-core fiber and twin-core fiber. J. Lightwave Technol. **27**(20), 5235–5239 (2009)
20. A.W. Snyder, W.R. Young, Modes of optical waveguides. J. Opt. Soc. Am. **68**(3), 297–309 (1978)

21. X. Zhang Hao, D. Ling-Yun, L. Yao, Y. Ling, L. Li-Hui, Y. Shu-Zhong, K. Gui-Yun, D. Xiao-Yi, A room-temperature, multi-wavelength erbium-doped fiber laser by exploiting polarization hole burning. Chin. Phys. Lett. **22**(1), 122–124 (2005)
22. J. Hernandez-Cordero, V.A. Kozlov, A.L.G. Carter, T.F. Morse, Fiber laser polarization tuning using a Bragg grating in a Hi-Bi fiber. IEEE Photonics Technol. Lett. **10**(7), 941–943 (1998)
23. Jefferson L. Wagener, D.G. Falquier, M.J.F. Digonnet, H.J. Shaw, A Mueller matrix formalism for modeling polarization effects in erbium-doped fiber. J. Lightwave Technol. **16**(2), 200–206 (1998)